



Origin of C type adakite magmas in the NE Xing'an block, NE China and tectonic implication

Changzhou Deng¹ · Guangyi Sun^{2,3} · Deyou Sun¹ · Hu Huang⁴ ·
Jianfeng Zhang⁵ · Jun Gou¹

Received: 11 March 2017 / Revised: 10 May 2017 / Accepted: 9 June 2017 / Published online: 21 June 2017
© Science Press, Institute of Geochemistry, CAS and Springer-Verlag GmbH Germany 2017

Abstract In this paper, we report new whole-rock geochemical and zircon U–Pb data for monzogranites in the NE Xing'an block. These data constrained the petrogenesis of C type (high Sr/Y) adakitic rocks and showed the spatial extent of the influence of the Mongol-Okhostk ocean tectonic regime and the collision between the Jiamusi Massif and Songliao Terrane. New zircon laser-ablation inductively coupled plasma mass spectrometry (LA-ICP-MS) U–Pb data indicated that the monzogranites in the studied area were emplaced in the Early Jurassic (~180 Ma). These rocks were characterized by unusually high SiO₂ (≥ 67.49), and Sr (461–759 ppm), but strikingly low Y (4.63–8.06 ppm) and HREE ($\sum \text{HREE} = 3.83\text{--}6.49$ ppm, Yb = 0.5–0.77 ppm) contents, with therefore high Sr/Y (67.2–119) and (La/Yb)_N (29.7–41.5) ratios, showing the geochemical characteristics of C type adakitic granite. The data displayed negligible Eu anomalies ($\text{Eu/Eu}^* = 0.77\text{--}1.08$), LREE-enriched and pronounced negative Nb and Ta anomalies. The C-type

adakites in the studied area were most likely derived from the partial melting of a thickened lower continental crust. The magma source is most likely dominated by amphibolites and garnet amphibolites. In combination with previously-reported data from igneous rocks from the Mesozoic in NE China, we conclude that the Xing'an block was influenced by the Mongol-Okhotsk subduction tectonic system, and experiences compressive settings from the amalgamation of the Jiamusi block in the east of the CAOB.

Keywords C type adakite · Geochemistry · U–Pb age · Thickened LCC · NE Xing'an block

1 Introduction

As initially defined (Defant and Drummond 1990; Martin 1999), adakites are defined as a kind of intermediate to felsic volcanic rocks formed in the arc setting, that show geochemical characteristics of SiO₂ ≥ 56 wt%, high Na₂O contents (3.5 wt% \leq Na₂O \leq 7.5 wt%), high La/Yb and Sr/Y ratios, and a strong depletion in high field strength elements (HFSE), Yb and Y. They are further classified into high-SiO₂ adakites and low-SiO₂ adakites by Martin et al. (2005), and are thought to be generated from the partial melting of metabasaltic rocks at relatively high pressure, with eclogites or amphibolites in the residual (see e.g. Moyen and Stevens 2006; Rapp and Watson 1995; Wolf and Wyllie 1994). Subsequently, continental (C) type (high Sr/Y) adakite was defined by Zhang et al. (2001) to describe intermediate to felsic magmatic rocks generated in continental settings in eastern China, which have similar geochemical characteristics to the typical adakite. This kind of adakite-like igneous rocks is widely reported in cratons (Zhang et al. 2001; Gao et al. 2004; Xu et al.

Changzhou Deng and Guangyi Sun have contributed equally to this work.

✉ Deyou Sun
sundy@jlu.edu.cn

¹ College of Earth Sciences, Jilin University, Changchun 130061, China

² State Key Laboratory of Environmental Geochemistry, Institute of Geochemistry, Chinese Academy of Sciences, Guiyang 550002, China

³ University of Chinese Academy of Sciences, Beijing 100049, China

⁴ Institute of Sedimentary Geology, Chengdu University of Technology, Chengdu 610059, China

⁵ Heilongjiang Institute of Geological Survey, Harbin 150036, China

2002, 2006, 2008; Wang et al. 2007) and active continental margins (He et al. 2011; Yang et al. 2016; Zhou et al. 2016).

Though the petrogenesis of high Sr/Y type magmas is still open to debate, C-type adakite can preserve some imprints about the lower crust, which can be used to trace the composition of the lower crust and discuss the crust-mantle process (He et al. 2011). Because of their unique temperature and pressure formation conditions, C-type adakitic rocks can be potentially utilized as tectono-magmatic process indicators, which can be of vital importance in reconstructing past regional tectonic regimes (e.g. Yang et al. 2016; Zhou et al. 2016).

Northeast (NE) China is located in the eastern part of Central Asian Orogenic (CAOB), and its tectonic transformation and overprinting in the Mesozoic is highly controversial (Xu et al. 2013; Wu et al. 2011). There are different proposals on the timing of the transformation from the Paleo-Asian regime to the Circum-Pacific regime: 1) in the Triassic (HBGMR 1993; Zhao et al. 1996); 2) in the Early-Middle Jurassic (Sun et al. 2005; Wu et al. 2007; Pei et al. 2008; Zhou et al. 2009); 3) in the Early Cretaceous (He et al. 1998). In recent years, based on the studies of precise age data and whole-rock geochemistry from igneous rocks, the influence of the spatial and temporal extents of the tectonic regime in the Mesozoic have constrained to a certain degree. e.g., the volcanic rocks in the Erguna massif are related to the subduction of the Mongol-Okhotsk oceanic plate, and those in the eastern Jilin-Heilongjiang provinces are related to the subduction of the Paleo-Pacific plate, the effect of the Mongol-Okhotsk suture belt on NE China was mainly in the Early Jurassic, Middle-late Jurassic and Early Cretaceous (Xu et al. 2013). The generation of the massive Triassic-Jurassic granitoids in the Erguna massif is related to the evolution of the Mongol-Okhotsk ocean (Wu et al. 2011). In general, Triassic-Jurassic granitoids in the Erguna Massif resulted from the southward subduction of the Mongol-Okhotsk ocean. Early-Middle Jurassic granitoids, with an age range of 210–155 Ma, were considered to be formed under the tectonic setting of subduction and collision between the Jiamusi Massif and Songliao Terrane (Wu et al. 2011). However, many studies up to now have focused on the normal (generally low Sr/Y) igneous rocks, while few studies have been paid attention on the C-type (high Sr/Y) granitoids in Xing'an block, NE China. Importantly, the Early Jurassic geodynamic setting of the Xing'an block are poorly constrained.

In this contribution, we focus on the Early Jurassic intrusive rocks at the northeast (NE) margin of the Xing'an block, NE China, and present zircon U-Pb and geochemical data, with the aim of constraining the petrogenesis of C

type adakite in this area. We also use this data to discuss the tectonic implication of the C type magma generation.

2 Geological setting and sample descriptions

2.1 Geological setting

The tectonic evolution of the Xing'an-Mongolia orogenic belt (the eastern part of the CAOB) is characterized by the amalgamation of multiple microcontinental blocks during the Phanerozoic (Sengör et al. 1993; Xiao et al. 2003; Li 2006; Wu et al. 2011, 2012). The northeastern part of this belt is divided into the Erguna, Xing'an, Songnen, and Jiamusi blocks from northwest to southeast, separated by the Tayuan-Xiguitu fault zone, the Hegenshan-Heihe fault zone, and the Mudanjiang fault zone, respectively (Fig. 1a). The Erguna block has remained stable since the Early Paleozoic (Ge et al. 2005; Wu et al. 2005). During the Middle Paleozoic, the Xing'an block accreted onto the Erguna block along the Tayuan-Xiguitu fault zone (She et al. 2012). The Songnen block collided with the joined Xing'an and Erguna blocks along the Hegenshan-Heihe fault zone during the late Paleozoic (Wu et al. 2002), and the Jiamusi terrane collided with these blocks along the Mudanjiang fault zone in the Early Mesozoic (Ge et al. 2007). Our studied region is located in the northeast section of Xing'an block (Fig. 1a), and the southeast section of the Tayuan-Xiguitu fault zone.

The studied area has experienced multiple tectonic movements, and is characterized by a series of E-W, NNE-SSW and NNW-SSE to NW-SE trending faults. Outcropping strata in the region consist mainly of Neoproterozoic, Cambrian, upper Silurian-Middle Devonian and Cretaceous units. The Neoproterozoic Xinghuadukou Group is composed of metamorphic intermediate-mafic submarine volcanic rocks, amphibolites, felsic gneisses, and marble (Zhou et al. 2011). The Cambrian Hongshenggou Formation consists of submarine limestone and light metasedimentary rocks. The Silurian-Devonian Niqiuhe Formation consists of marine facies volcanic rocks, clastic rocks, carbonates and radiolarian-bearing siliceous formations. The Mesozoic outcrops are mainly Early Cretaceous volcanic formations consisting of a suit of subducted-related basalt-andesite-rhyolite volcanic rocks.

2.2 Occurrence and petrography

Lacking precious age data, the intrusion rocks in Xing'an block were mapped as Late Proterozoic to Paleozoic granites (HBGMR 1993). However, recent U-Pb isotopic studies indicate that Proterozoic rocks are quite restricted

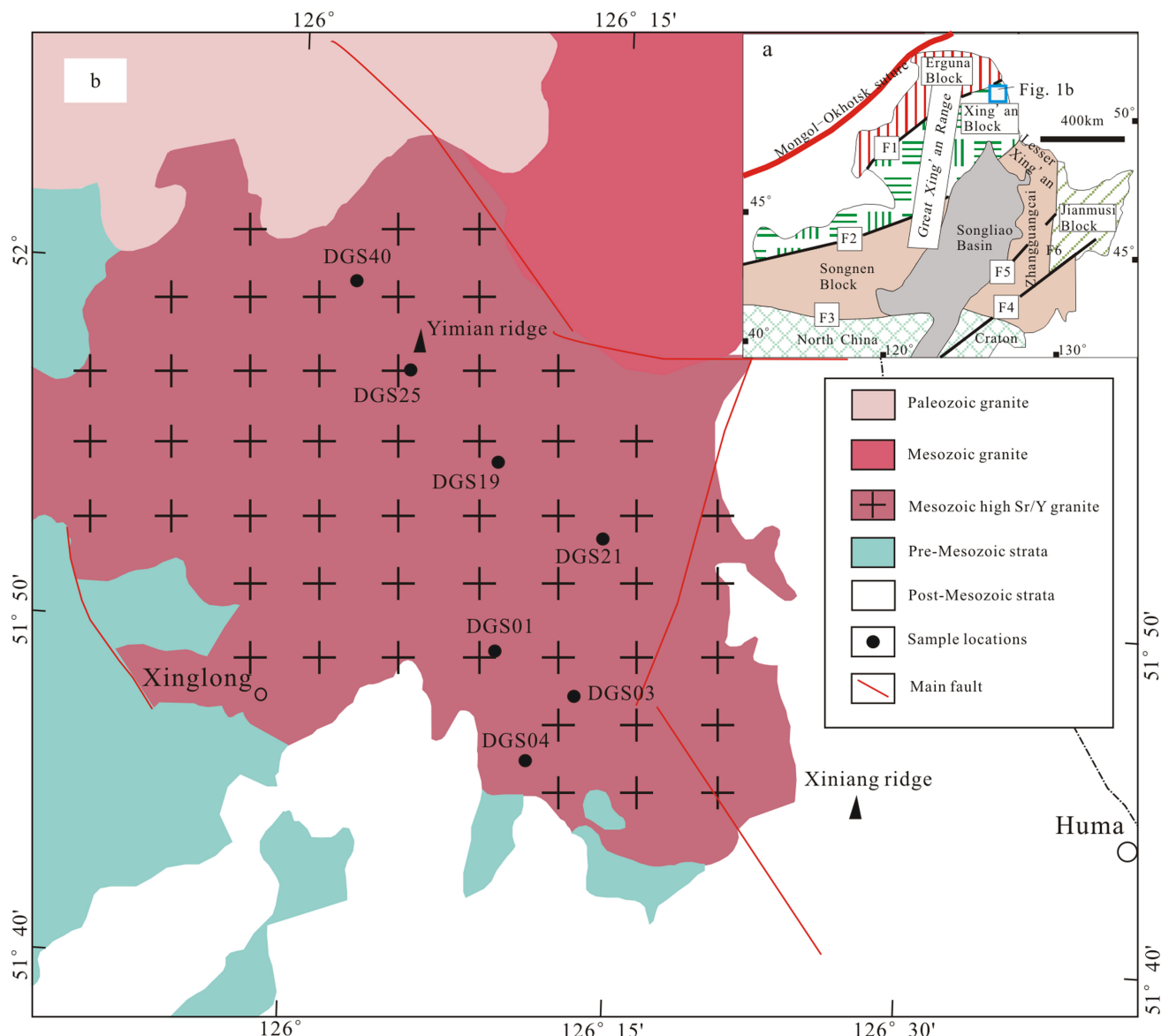


Fig. 1 Tectonic location map (after Hu et al. 2014) (a), *F1* Tayuan–Xiguít fault; *F2* Hegenshan–Heihe fault; *F3* Chifeng–Kaiyuan fault; *F4* Dunhua–Mishan fault; *F5* Yitong–Yilan fault; *F6* Jiayin–Mudanjiang fault. And simplified regional geological map of NE Xing'an block

and many so-called Precambrian granites are actually Early Paleozoic granitoids (Sui et al. 2007; Wu et al. 2011). But by far the most components of intrusion rocks in this region are granites that emplaced during the Late Triassic to Early Jurassic (Wu et al. 2011).

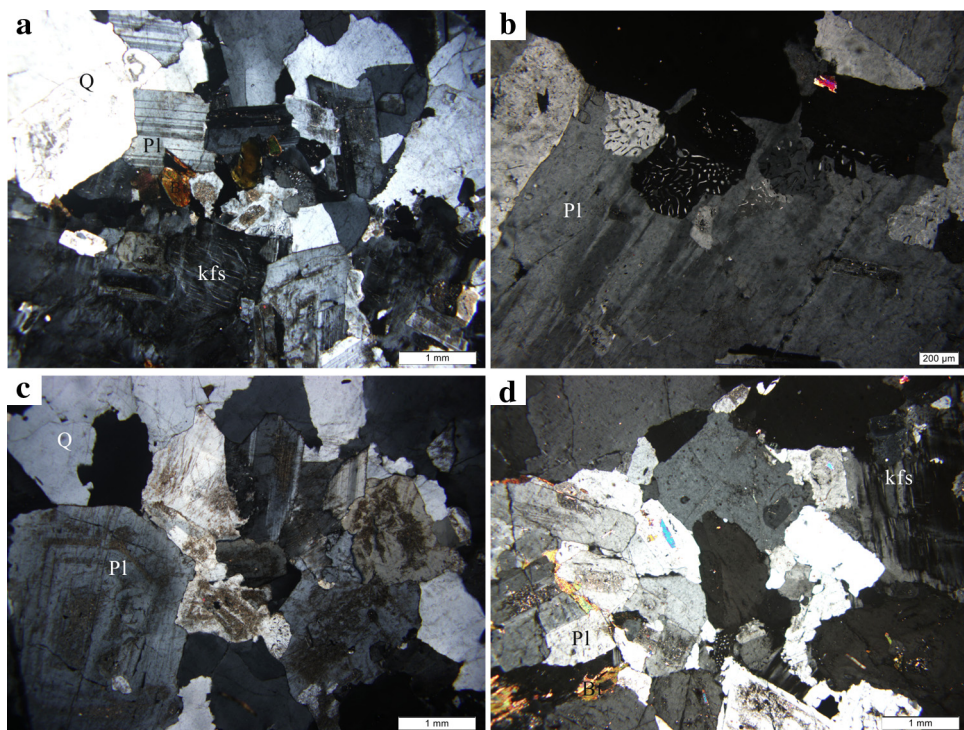
In this paper, samples from the Early Jurassic Diyingzi batholith in the NE Xing'an block were collected. The Diyingzi batholith, with an area of $\sim 1000 \text{ km}^2$, crops out in the northern section of the Xinglong town (Fig. 1b), and is dominated by monzogranites (sample DGS19, N $51^{\circ}54'20''$, E $126^{\circ}09'15''$), with minor amounts of diorite veins and porphyry granite. It intrudes into the Neoproterozoic, Cambrian, and Ordovician strata, and is overlain by Early Cretaceous volcanic rocks. The monzogranite shows

coarse-medium grained crystalline texture, massive structure, and consists of 20%–30% plagioclase, 35%–40% K-feldspar, 25%–30% quartz, and 5% biotite. Anhedral quartz grains show undulatory extinction, the plagioclase and K-feldspar is generally automorphic and subhedral crystal, and the former is twinned (Fig. 2). Accessory minerals include zircon and magnetite.

3 Analytical methods

We selected 7 monzogranite samples for whole rock geochemical study, and the sample DGS19 was also used for zircon U–Pb dating analysis. All samples represent

Fig. 2 Microphotographs of representative monzogranite samples in NE Xing'an block. *Pl* Plagioclase; *Kfs* K-feldspar; *Q* Quartz; *Bt* Biotite



extremely rare examples of unaltered, fresh and undeformed igneous rocks. The sampling locations are shown in Fig. 1.

All whole-rock major elements were analyzed using X-ray fluorescence at the State Key Laboratory of Geological Processes and Mineral Resources, China University of Geosciences, Wuhan. The analytical uncertainty is generally <5%. Trace element analyses were performed in Wuhan Sample Solution Analytical Technology Co., Ltd (WSSATCL), and trace element concentrations were determined using a Thermo-Finnigan element inductively coupled plasma mass spectrometer (ICP-MS) after HNO_3 -HF digestion of about 50 mg of the sample powder in a Teflon vessel at 190 °C. Analytical accuracy and precision were monitored by Chinese national reference GSR1 (granite), GSR2 (andesite) and GSR3 (basalt). The precision is 5% of the quoted values for elements present less than 1 ppm. Accuracy is estimated to be better than 5% for the reported values. The detailed sample-digesting procedure for ICP-MS analyses and analytical precision and accuracy for trace elements are the same as described by Liu et al. (2008).

Zircon grains were separated using conventional magnetic and density techniques. Zircon grains were hand-picked under a binocular microscope, mounted in an epoxy resin 1 inch in diameter, and polished to expose the centers of zircon grains. Prior to analytical work, all zircon grains were examined under a microscope with transmitted and reflected light, as well as Cathodoluminescence (CL) images

using a scanning electron microscope to reveal their internal structures at WSSATCL. LA-ICP-MS zircon U-Pb dating and trace element were analyzed at WSSATCL. Detailed operating conditions for the laser ablation system and the ICP-MS instrument and data reduction are the same as the description by Liu et al. (2010). Zircon 91,500 was used as an external standard for U-Pb dating, and was analyzed twice every 5 analyses. Preferred U-Th-Pb isotopic ratios used for 91,500 are from Wiedenbeck et al. (1995). Uncertainty of preferred values for the external standard weighted mean calculations were made using Isoplot/Ex_ver3 (Ludwig 2003).

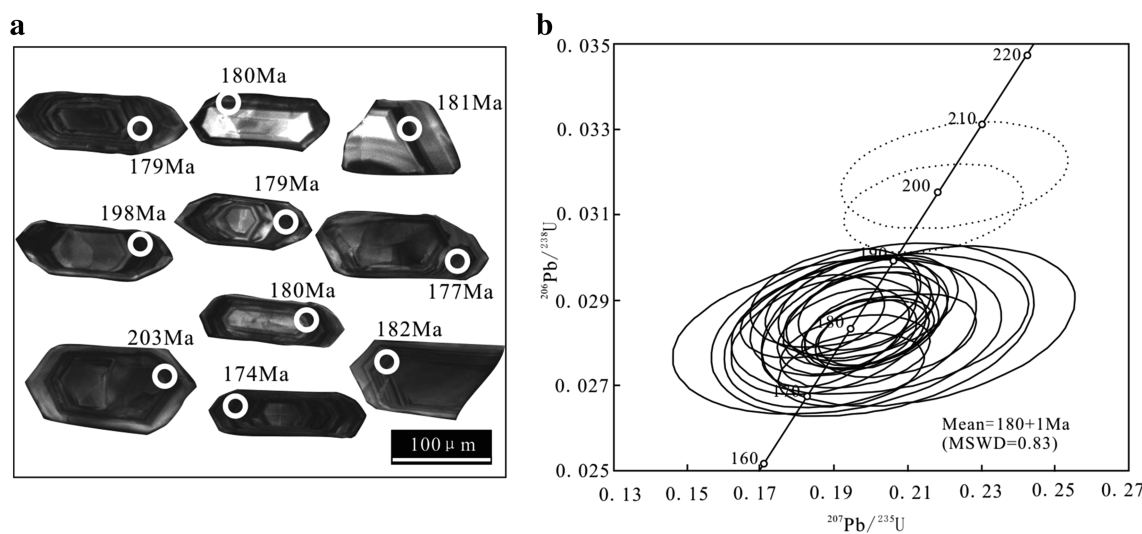
4 Results

4.1 U-Pb zircon age

Sample DGS19 from the NE Xing'an block were selected for LA-ICP-MS zircon U-Pb dating. The results are listed in the Table 1. Representative zircon CL images and their U-Pb Concordia plots are shown in Fig. 3. Zircons from the magmatic rocks are characterized by light yellow to colorless, euhedral, and long to short prismatic forms. The crystals range in length from 65 to 200 μm , with length/width ratios ranging from 2:1 to 3:1. Most zircons show obvious oscillatory zoning on the CL images (Fig. 3a). Zircon grains have variable U and Th contents of 73.7–1122 and 39.8–702 ppm, respectively. The relatively

Table 1 LA-ICP-MS zircon U–Pb dating for the monzogranite samples in the NE Xing'an block

Spot no.	Pb ppm	Th ppm	U ppm	Th/U	Isotopic ratios						Ages (Ma)					
					$^{207}\text{Pb}/^{206}\text{Pb}$		$^{207}\text{Pb}/^{235}\text{U}$		$^{206}\text{Pb}/^{238}\text{U}$		$^{207}\text{Pb}/^{206}\text{Pb}$		$^{207}\text{Pb}/^{235}\text{U}$		$^{206}\text{Pb}/^{238}\text{U}$	
					Ratio	1σ	Ratio	1σ	Ratio	1σ	Age	1σ	Age	1σ	Age	1σ
1	21.01	180	584	0.31	0.0500	0.0022	0.1966	0.0081	0.0286	0.0004	195	97	182	7	182	3
2	3.59	134	73.3	1.84	0.0528	0.0053	0.2001	0.0180	0.0283	0.0008	320	264	185	15	180	5
3	41.8	702	1067	0.66	0.0512	0.0016	0.2004	0.0061	0.0282	0.0003	250	66	185	5	179	2
4	2.84	39.8	73.7	0.54	0.0585	0.0062	0.2126	0.0174	0.0284	0.0008	550	231	196	15	180	5
5	17.52	343	428	0.80	0.0535	0.0024	0.2064	0.0089	0.0282	0.0004	350	104	191	8	179	2
6	26.15	319	750	0.43	0.0489	0.0019	0.1911	0.0087	0.0285	0.0006	143	90	178	7	181	4
7	42.1	626	1122	0.56	0.0502	0.0016	0.1965	0.0064	0.0282	0.0003	206	76	182	5	179	2
8	23.35	446	605	0.74	0.0491	0.0019	0.1921	0.0073	0.0283	0.0004	150	91	178	6	180	3
9	4.57	51.2	127	0.40	0.0523	0.0046	0.2020	0.0165	0.0284	0.0007	298	204	187	14	181	4
10	27.55	380	755	0.50	0.0510	0.0020	0.1999	0.0075	0.0283	0.0004	243	89	185	6	180	2
11	24.93	400	662	0.60	0.0501	0.0028	0.1989	0.0100	0.0289	0.0005	198	131	184	8	183	3
12	14.23	275	366	0.75	0.0505	0.0024	0.1981	0.0091	0.0285	0.0005	217	111	184	8	181	3
14	12.28	165	332	0.50	0.0478	0.0024	0.1901	0.0095	0.0290	0.0005	87	124	177	8	185	3
15	9.64	117	272	0.43	0.0495	0.0029	0.1938	0.0110	0.0286	0.0006	172	139	180	9	182	3
16	31.41	504	850	0.59	0.0508	0.0022	0.1954	0.0083	0.0278	0.0003	232	102	181	7	177	2
17	5.38	166	118	1.41	0.0518	0.0043	0.1940	0.0140	0.0282	0.0007	280	191	180	12	179	5
18	3.32	41.9	97.4	0.43	0.0495	0.0050	0.1905	0.0182	0.0281	0.0007	172	222	177	16	179	5
19	29.68	592	784	0.76	0.0511	0.0018	0.1992	0.0072	0.0283	0.0003	256	79	184	6	180	2
20	10.11	162	276	0.59	0.0505	0.0032	0.1881	0.0108	0.0282	0.0006	217	153	175	9	179	4
21	23.83	302	679	0.44	0.0467	0.0020	0.1837	0.0080	0.0286	0.0004	32	168	171	7	182	2
22	11.47	97.7	339	0.29	0.0492	0.0025	0.1946	0.0096	0.0289	0.0005	167	149	181	8	183	3
24	24.13	299	698	0.43	0.0497	0.0018	0.1980	0.0074	0.0288	0.0004	189	85	183	6	183	2
25	25.52	512	712	0.72	0.0514	0.0021	0.1944	0.0081	0.0274	0.0003	257	92	180	7	174	2
13	18.98	204	481	0.42	0.0504	0.0024	0.2167	0.0100	0.0311	0.0004	213	111	199	8	198	3
23	13.36	94.1	352	0.27	0.0507	0.0030	0.2224	0.0126	0.0319	0.0005	228	142	204	10	203	3

**Fig. 3** Representative zircon CL images (a), and concordia diagram of zircon U–Pb ages (b) for monzogranite samples from the NE Xing'an block. Dashed ellipses are not included in the age calculation. Ellipses represent 1-sigma uncertainty for individual analyses

high Th/U ratios (0.27–1.84), together with the clear oscillatory zoning, indicate a magmatic origin (Williams and Claesson 1987; Kinny et al. 1990; Koschek 1993; Corfu et al. 2003).

Twenty-three spots yield $^{206}\text{Pb}/^{238}\text{U}$ ages between 174 and 185 Ma, with a weighted mean age of 180 ± 1 Ma (MSWD = 0.83) (Fig. 3b), which could be interpreted to be the emplacement age of the granite intrusion in our study area. Two other spots give slightly old $^{206}\text{Pb}/^{238}\text{U}$ ages 198 and 203 Ma, which could be interpreted as the xenocrystic grains incorporated into the granite magma.

4.2 Major and trace elements

The monzogranite samples contain SiO_2 of 67.49 wt%–72.31 wt%. Their Na_2O and K_2O contents range from 4.20 wt% to 5.24 wt% and from 2.88 wt% to 3.66 wt%, respectively, with $\text{K}_2\text{O}/\text{Na}_2\text{O}$ ratios of 0.55–0.85. The samples contain Al_2O_3 of 14.30 wt%–16.40 wt%, relatively low CaO of 1.62 wt%–2.53 wt%, showing moderately peraluminous signatures (Fig. 4a). They have $\text{Fe}_2\text{O}_3\text{T}$ contents of 1.1 wt%–2.6 wt% and MgO of 0.39 wt%–0.96 wt%, with $\text{Mg}\#$ values of 40–46. They plot in or near the field of high-K calc-alkline in the SiO_2 – K_2O diagram (Fig. 4b).

The samples are low in total REEs (96.29–143.22 ppm), and exhibit LREE enrichment and HREE depletion in chondrite-normalized REE patterns [$(\text{La/Yb})_N = 29.75\text{--}41.53$, $(\text{Dy/Yb})_N = 1.31\text{--}1.78$], with negligible Eu ($\text{Eu/Eu}^* = 0.77\text{--}1.08$, with an average value of 0.94) anomalies (Fig. 5a). These samples show strong enrichments in large ion lithophile elements (LILE), such as Rb, Ba, Th and U, and depletion in high field strength elements (HFSE), such as Nb, Ta and Ti (Fig. 5b), which exhibit typical subduction-related geochemical characteristics (Innocenti et al. 2005).

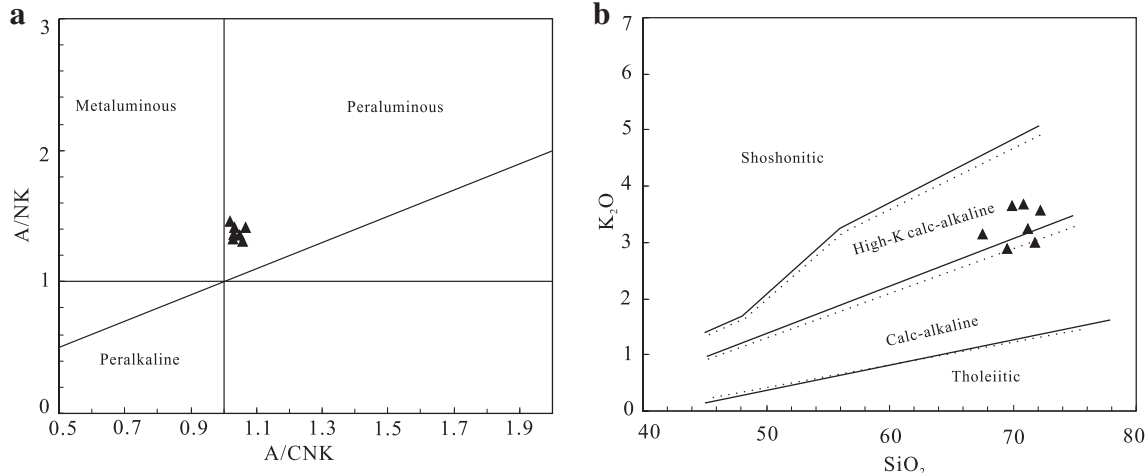


Fig. 4 **a** A/NK (molar $\text{Al}_2\text{O}_3/[\text{Na}_2\text{O} + \text{K}_2\text{O}]$) versus A/CNK (molar $\text{Al}_2\text{O}_3/[\text{CaO} + \text{Na}_2\text{O} + \text{K}_2\text{O}]$) diagram (Maniar and Piccoli 1989) for monzogranite samples in NE Xing'an block. **b** SiO_2 versus K_2O diagram (Peccerillo and Taylor 1976) for monzogranite samples in NE Xing'an block

5 Discussion

5.1 Petrogenesis

The seven samples are characterized by prominently high SiO₂ (≥ 67.49), and Sr (461–759 ppm), but low Y (4.63–8.06 ppm) and HREE ($\sum \text{HREE} = 3.83\text{--}6.49$ ppm, Yb = 0.5–0.77 ppm) contents, with therefore high Sr/Y (67.2–119) and (La/Yb)_N (29.7–41.5) ratios, showing geochemical characteristics of C type adakitic granite. In the two widely used (La/Yb)_N versus Yb_N (Martin 1999), and Sr/Y versus Y (Defant and Drummond 1990) discrimination diagrams, all samples plot into the field of adakite (Fig. 6). Several models have been proposed for the petrogenesis of the granitoid rocks with high Sr/Y geochemical signature: assimilation fractional crystallization (AFC) processes of mantle-derived magmas (Castillo et al. 1999; Liu et al. 2003; Macpherson et al. 2006), partial melting of subducted oceanic slabs (Defant and Drummond 1990; Rapp et al. 1999), magmas mixing between felsic and basaltic magmas (Streck et al. 2007), partial melting of delaminated (Kay and Kay 1993; Xu et al. 2002) or thickened (Chung et al. 2003; Long et al. 2015; Zhou et al. 2016) lower continental crust (LCC).

Adakitic rocks generated by AFC processes of basaltic magmas usually contain amphibole or clinopyroxene minerals and require volumes of basaltic to dacitic rocks (Castillo et al. 1999; Macpherson et al. 2006). In the field, no coeval mafic to intermediate rocks have been found in the NE Xing'an block, combined with the absence of amphibole and clinopyroxene minerals in the samples, and the lack of mafic xenoliths, precluding their derivation from the basaltic magma by AFC processes or magma mixing. Moreover, the lack of strong correlations between

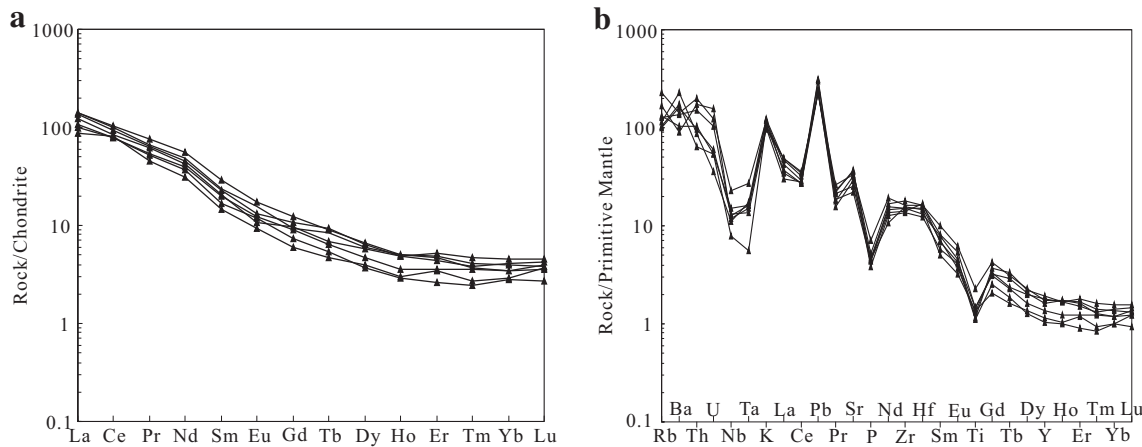


Fig. 5 Chondrite-normalized REE pattern (a) and Primitive mantle-normalized trace element variation diagrams (b) for monzogranite samples in NE Xing'an block. Normalizing values are from Sun and McDonough (1989)

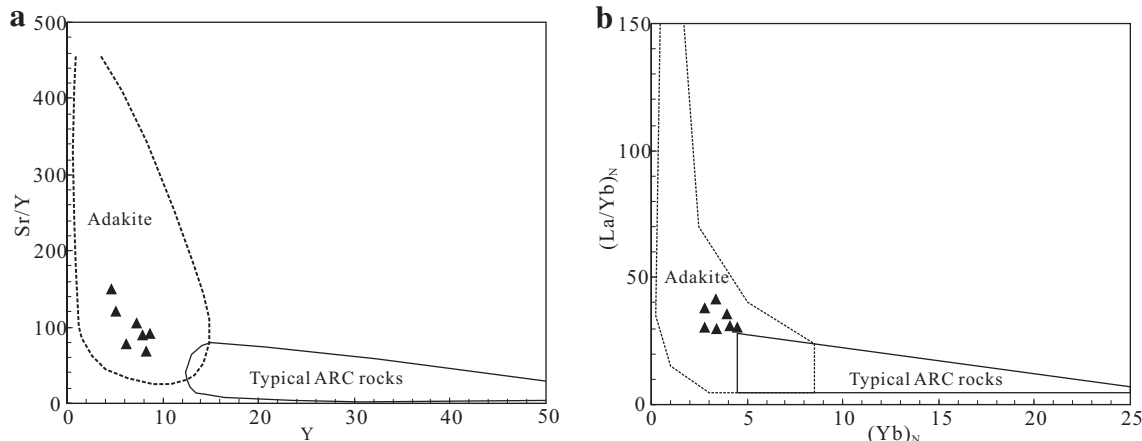


Fig. 6 a Sr/Y versus Y diagram (Defant and Drummond 1990) and b (La/Yb)_N versus Yb_N diagram (Martin 1986) for monzogranite samples in NE Xing'an block

Sr/Y, La/Sm, (La/Yb)_N, Zr/Nb and Nb/Ta ratios and SiO₂ contents preclude fractionation.

Due to the subsequent interaction with overlying mantle peridotite during the magma ascent, delaminated lower crust or oceanic slab-derived adakitic rocks generally have the geochemical feature of high Cr (≥ 20 ppm) and Ni (≥ 12 ppm) values (Martin 1999; Xu et al. 2002; Martin et al. 2005). However, the NE Xing'an adakitic granites are characterized by dominantly low Cr (1.27–3.94 ppm), and Ni (1.28–3.33 ppm) contents. In addition, they have Rb/Sr ratios of 0.08–0.23, higher than those (< 0.05) of slab-derived adakites (Huang et al. 2009), and show high SiO₂ contents. These geochemical features rule out an origin from the partial melting of a subducted ocean slab or delaminated lower crust.

The studied samples with low Mg# (40.3–46.2), MgO (0.39 wt%–0.96 wt%) (Fig. 7a, b) values, as well as low Rb/Ba (0.05–0.17), and Rb/Sr (0.08–0.27) ratios (Fig. 7c),

have typical features of lower continental crust (Rudnick and Gao 2003). In addition, adakitic rocks in the present study exhibit diagnostic characteristics of low Ni and Cr contents (Fig. 7d, e), indicating that its magmatic protolith was most probably derived from the partial melting of lower crustal materials.

5.2 Source characteristics

The source of C type adakitic granitoid rocks are also highly debated because these geochemical signatures can be produced by multiple lower continental crust sources. Several studies suggest that C type (high Sr/Y) adakitic can be derived from amphibolites, ecogites, gneisses or granulites (Zhang et al. 2001; Ge et al. 2002; Xu et al. 2006, 2013; Wang et al. 2007). The geochemical feature of the C type adakite in this contribution indicate that the Early Jurassic monzogranites in NE Xing'an block were

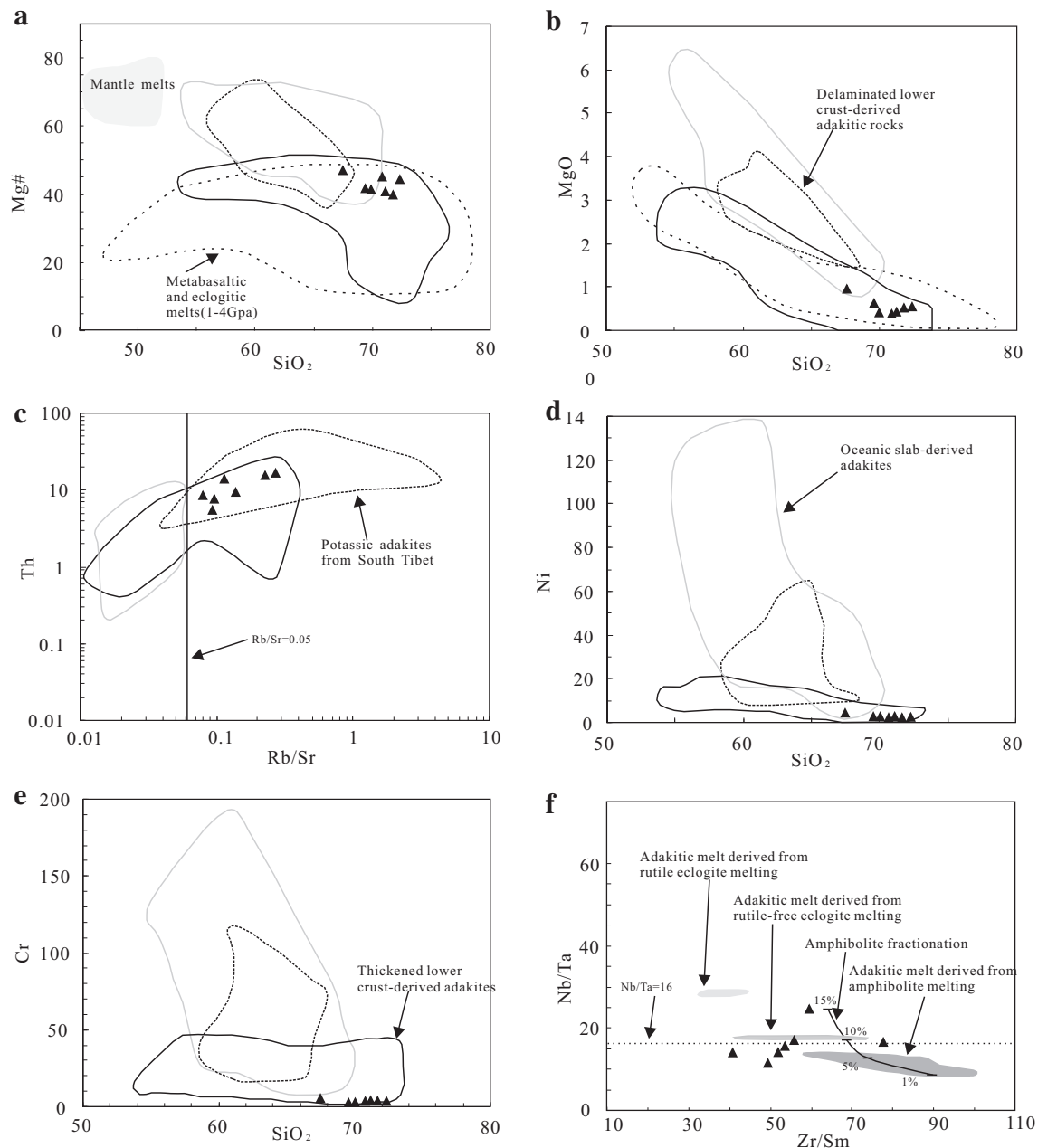


Fig. 7 a Mg# versus SiO₂ diagram (Long et al. 2015), b–e MgO versus SiO₂, Th versus Rb/Sr, Ni versus SiO₂, and Cr versus SiO₂ diagrams (Huang et al. 2009), f Nb/Ta versus Zr/Sm diagrams (Long et al. 2015) for adakitic rocks from NE Xing'an block. Major oxides are in wt%, and trace elements are in ppm

generated by the partial melting of amphibolite and garnet amphibolite in a thickened lower continental crust setting, as discussed below.

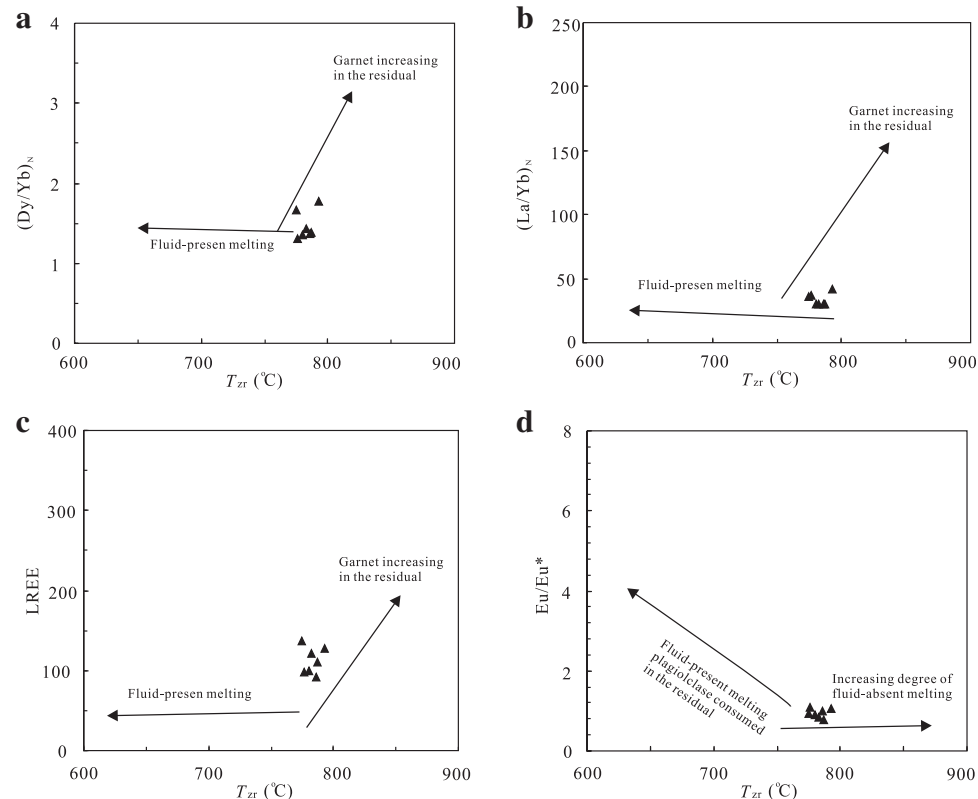
Many studies have proposed that both amphibole and garnet as residuals in the magma source can generate high Sr/Y and La/Y ratio melts (Davidson et al. 2007; Macpherson et al. 2006). The fact that HREE and Y have high garnet-melt partition coefficients means that residual garnet generally result in geochemical features of depletion in HREE and Y. And previous studies show that partial

melting of a thickened lower continental crust with residual garnet will generate melts with $(\text{Ho}/\text{Yb})_{\text{N}} > 1.2$, $\text{Y}/\text{Yb} > 10$ and high $(\text{Dy}/\text{Yb})_{\text{N}}$ value (Ge et al. 2002; Hu et al. 2012). The geochemical feature that amphibole preferentially incorporates, MREE, means that hornblende in the residual will generate melts with flat HREE patterns with $\text{Y}/\text{Yb} \approx 10$, $(\text{Ho}/\text{Yb})_{\text{N}} \approx 1$ and relatively low $(\text{Dy}/\text{Yb})_{\text{N}}$ value (Ge et al. 2002; Hu et al. 2012). The Early Jurassic C type adakites have Y/Yb , $(\text{Ho}/\text{Yb})_{\text{N}}$ and $(\text{Dy}/\text{Yb})_{\text{N}}$ ratios of 9.56–12.59 (with an average value of 11.07),

1.02–1.49 (with a average value of 1.16), and 1.31–1.77 (with a average value of 1.47), respectively. This indicates that both amphibole and garnet were residual within the source of these adakitic magmas, consistent with their low Nb/Ta (11.7–24.2, with an average value of 15.9) and high Zr/Sm (40.9–78, with an average value of 55.5) ratios (Fig. 7f). Compared with the high Sr/Y group I granite in the SW Alxa block, Southern CAOB, which was generated by fluid-absent partial melting of mafic to intermediate rocks (Zhou et al. 2016), samples in this study have lower $(\text{Dy}/\text{Yb})_{\text{N}}$, $(\text{La}/\text{Yb})_{\text{N}}$ and LREE values (Fig. 8a–c), indicating relatively minor garnet in the residual. Meanwhile, the studied samples have higher zircon saturation temperatures (T_{zr} , calculated by Watson and Harrison 1983; the results show in Table 2) than high Sr/Y group II granite in SW Alxa block, which was derived from the partial melting of the crustal basement materials under fluid-present conditions (Zhou et al. 2016), suggesting a fluid-absent melting condition (Fig. 8d). In addition, the presence of residual garnet in magma sources also indicates that partial melting occurred in a thickened LCC (>50 km; Atherton and Petford 1993; Wang et al. 2007; Xu et al. 2013).

Most of the samples show relatively low Nb/Ta ratios (Fig. 7f), which support amphibolite melting, but not eclogite melting. Besides, predominant amphiboles in the residual preclude the possibility of granulitic or gneissic source, which mainly consist of plagioclases and quartzes.

Fig. 8 Variation of **a** $(\text{Dy}/\text{Yb})_{\text{N}}$, **b** $(\text{La}/\text{Yb})_{\text{N}}$, **c** LREE and **d** Eu/Eu^* versus zircon saturation temperature (T_{zr}) (calculated by Watson and Harrison 1983). Major oxides are in wt%, and trace elements are in ppm



Furthermore, the relatively low Rb/Ba and Rb/Sr ratios of the C-type adakitic samples indicate derivation from basaltic sources (Fig. 9; Sylvester 1998). Thus, it appears plausible for the NE Xing'an block adakitic granite samples to have been formed by the partial melting of a lower-crustal metabasaltic source.

5.3 Tectonic implications

Magmatic-type zircons from the NE Xing'an block adakitic granite yield consistent ages of 180 Ma, representing the crystallization age of the adakitic rocks. They exhibit typical subduction-related geochemical characteristics (Fig. 5) and dominantly plot into the volcanic arc granite (VAG) and late-orogenic fields (Fig. 10a–c, Pearce et al. 1984; Batchelor and Bowden 1985). Combined with the occurrence of 180 Ma calc-alkaline volcanic arc granitoids in the Xing'an block (Sui et al. 2007; Wu et al. 2011), the NE Xing'an block most likely developed as a continental arc during the early Jurassic time, with the subduction-related geochemical features of the adakitic rocks inherited from lower-crustal sources. The formation of the early Jurassic adakitic rocks in the studied region can be reasonably explained by an oceanic subduction system located in the north of the NE Xing'an continental arc, which was possibly thickened in a compressional environment.

Table 2 Major element (wt%) and trace element (ppm) for samples from NE Xing'an block

Sample	DGS01	DGS03	DGS04	DGS19	DGS21	DGS25	DGS40
SiO ₂	69.59	71.74	70.82	71.14	69.92	72.31	67.49
TiO ₂	0.32	0.30	0.28	0.24	0.25	0.32	0.49
Al ₂ O ₃	16.40	15.13	15.93	15.28	16.17	14.30	16.11
Fe ₂ O ₃ T	1.88	1.74	1.10	1.43	1.42	1.60	2.60
MnO	0.05	0.05	0.03	0.05	0.04	0.05	0.05
MgO	0.56	0.50	0.39	0.42	0.42	0.55	0.96
CaO	2.26	1.91	1.62	1.87	2.01	1.65	2.53
Na ₂ O	5.24	4.82	5.00	4.55	4.76	4.20	4.79
K ₂ O	2.88	2.99	3.62	3.24	3.66	3.57	3.10
P ₂ O ₅	0.11	0.10	0.10	0.08	0.10	0.10	0.16
LOI	0.50	0.60	0.92	1.20	0.79	0.79	0.90
K ₂ O/Na ₂ O	0.55	0.62	0.72	0.71	0.77	0.85	0.65
Mg#	41	40	45	40	41	44	46
A/CNK	1.03	1.03	1.06	1.06	1.05	1.04	1.02
AR	2.54	2.69	2.93	2.66	2.73	2.90	2.47
Cr	1.31	1.39	1.61	1.33	1.27	1.93	3.94
Co	2.34	2.03	1.62	2.28	1.78	2.62	4.89
Ni	1.40	1.28	1.33	1.66	1.57	1.83	3.33
Rb	63.2	83.2	146.5	64.9	73.8	106.9	80.1
Sr	759	610	542	684	770	461	702
Y	7.25	5.15	8.06	4.63	8.69	6.11	7.94
Zr	200	175	166	152	170	157	180
Nb	9.41	10.83	16.53	5.62	7.94	8.58	9.11
Ba	1140	733	994	1212	1587	630	937
La	33.35	20.97	29.59	25.03	31.83	24.01	33.64
Ce	60.78	50.07	51.68	47.76	57.88	48.45	64.14
Pr	6.36	4.34	5.87	5.00	6.07	5.19	7.24
Nd	23.00	14.30	19.86	17.04	21.47	18.45	26.28
Sm	3.57	2.24	3.12	2.54	3.47	3.04	4.39
Eu	0.90	0.54	0.62	0.69	0.77	0.71	1.02
Gd	1.90	1.23	1.97	1.49	2.21	1.84	2.51
Tb	0.32	0.18	0.26	0.20	0.35	0.24	0.33
Dy	1.53	1.02	1.45	0.95	1.64	1.18	1.69
Ho	0.29	0.17	0.27	0.16	0.28	0.20	0.29
Er	0.77	0.57	0.74	0.44	0.86	0.59	0.80
Tm	0.10	0.07	0.10	0.06	0.12	0.09	0.11
Yb	0.58	0.50	0.70	0.48	0.77	0.58	0.68
Lu	0.10	0.09	0.11	0.07	0.12	0.09	0.10
Hf	4.98	4.50	4.65	3.79	4.12	5.11	5.01
Ta	0.55	0.66	1.09	0.23	0.71	0.62	0.66
Tl	0.40	0.49	0.96	0.40	0.45	0.72	0.55
Pb	15.98	17.17	21.89	16.21	16.39	21.47	16.21
Th	8.10	8.82	16.82	5.48	7.31	14.52	12.96
U	1.25	1.14	2.61	1.15	0.74	3.32	2.15
Y	7.25	5.15	8.06	4.63	8.69	6.11	7.94
Nb	9.41	10.83	16.53	5.62	7.94	8.58	9.11
ΣREE	133.53	96.29	116.33	101.93	127.83	104.68	143.22
ΣHREE	127.96	92.46	110.75	98.07	121.49	99.86	136.72
(La/Yb) _N	42	30	30	37	30	30	36
Eu/Eu*	1.05	1.00	0.77	1.08	0.85	0.91	0.94
(Dy/Yb) _N	1.77	1.36	1.38	1.31	1.43	1.36	1.66
Tzr	793	786	787	776	783	780	775

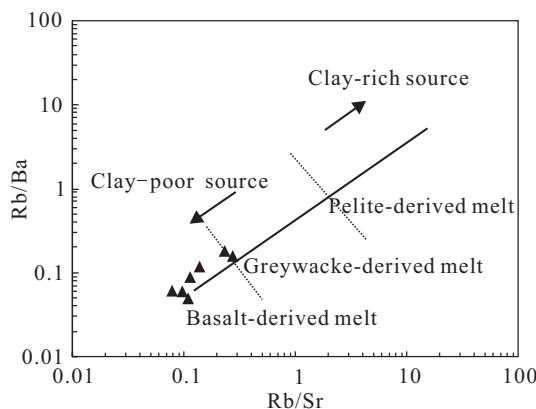


Fig. 9 Rb/Ba versus Rb/Sr discrimination diagrams (Sylvester 1998) for monzogranite samples in NE Xing'an block

As the NE Xing'an block was in a continental arc setting during the Early Jurassic time, the delamination of a thickened lower crust that typically occurs in post collisional extension settings seems unlikely. Ridge subduction-related adakitic rocks are always associated with high temperature magmatism, such as igneous charnockites and alkali-feldspar granites (Geng et al. 2009). Our calculation results show that the NE Xing'an block rocks yield T_{zr} of 775–793 °C, much lower than temperatures (≥ 900 °C) of magmatism generated by ridge subduction (Geng et al. 2009). Besides, all the T_{zr} values are slightly lower than the solidus (~ 820 –900 °C) for dehydration melting of amphibolites at low pressure. However, the solidus decline sharply at higher pressures (~ 10 –15 kbar, Moyen and Stevens 2006; Qian and Hermann 2013; Wyllie and Wolf 1993). All these features support a derivation of the monzogranite samples from a thickened lower continental crust, which suggests that there was a crust thickening event before Early Jurassic in NE Xing'an block, NE China.

In recent years, a growing number of evidence indicates that the Mesozoic magmatism in the Great Xing'an Range (GXAR) are related to the subduction of the Mongol-Okhotsk ocean. Firstly, Xu et al. (2013) suggested that the Early Jurassic igneous rocks in the Erguna massif are related to the subduction of the Mongol-Okhotsk oceanic plate, which was developed during the Late Paleozoic (Tomurtogoo et al. 2005) and closed in the Middle Jurassic (Kravchinsky et al. 2002; Tomurtogoo et al. 2005). Secondly, Zhang et al. (2010) proposed that Mesozoic igneous rocks show an Eastward-younging migration, coincident with the west to east closure direction of the Mongol-Okhotsk ocean (e.g., Zhao et al. 1990; Yin and Nie 1996; Tomurtogoo et al. 2005; Ying et al. 2010). Furthermore,

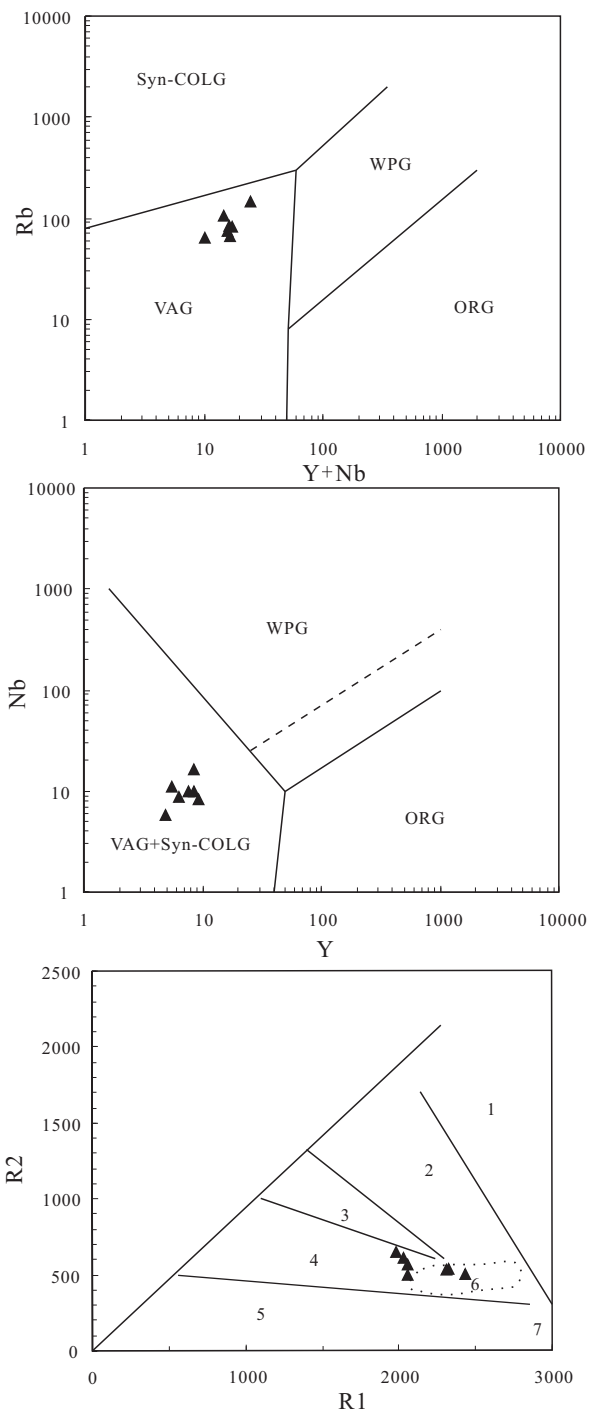


Fig. 10 Tectonic discrimination diagram for samples from the NE Xing'an block. Note that Nb versus Y and Rb versus ($Y + Nb$) diagrams are from Pearce et al. (1984), and R1–R2 diagram is from Batchelor and Bowden (1985). VAG volcanic arc granites, COLG collision granites, WPG within-plate granites, ORG ocean-ridge granites. 1 Mantle fractionation; 2 pre-plate collision; 3 post-collision uplift; 4 late-orogenic; 5 anorogenic; 6 Sy-collision; 7 post-orogenic. $R1 = 4Si - 11(Na + K) - 2(Fe + Ti)$; $R2 = 6Ca + 2Mg + Al$

previous research demonstrates that the Paleo-Pacific plate displayed Northward and North–North-Eastward subduction during the Jurassic–Early Cretaceous, and had negligible influence to East Asian continent until the Late Cretaceous (Maruyama and Send 1986). Thus, the subduction of the Paleo-Pacific ocean should have limited influence on the GXAR, which is located far away from the Paleo-Pacific margin in the east. Thus, we conclude that the igneous rocks are more plausibly related to the southward subduction of the Mongol-Okhotsk ocean. Meanwhile, another remarkable tectonic event is the collision between the Jiamusi Massif and Songliao Terrane in the Early Jurassic in the southeast section of the studied area (Zhou et al. 2009). The Jiamusi Massif, which might have been part of Gondwana (Wilde et al. 1997), is thought to be an accretionary Terrane, instead of a part of the CAOB, and have collided with the CAOB at ~185–166 Ma along the Mudanjiang fault zone (Wu et al. 2011). The amalgamation of the Jiamusi block with the CAOB might provide a sustained westerly-directed compressive tectonic setting, which overprint to the thickened crust in our studied area.

Briefly, the subducted-related geochemical features and crust thickening events in this study imply that Xing'an block was influenced by both the Mongol-Okhostsk ocean tectonic regime and collision between the Jiamusi Massif and Songliao Terrane. The onset of the westerly-directed compression of the amalgamation of the Jiamusi block with the CAOB, associated with southward subduction of the Mongol-Okhotsk ocean, resulted in the formation of C type adakite in NE Xing'an block.

6 Conclusions

Based on the study of whole rock major, trace elements and zircon U–Pb age data from monzogranite samples in NE Xing'an block, we draw the following conclusions:

1. The monzogranites in NE Xing'an block intruded at 180 Ma and showed geochemical features of C type adakitic rocks.
2. These C type adakitic rocks were most likely derived from the partial melting of a thickened lower continental crust, with dominant amphibole and minor garnet in the residual.
3. The subducted-related geochemical features imply that the Xing'an block was influenced by the Mongol-Okhotsk ocean tectonic regime, and experienced a compressive setting by the amalgamation of the Jiamusi block with the CAOB in Early Jurassic.

Acknowledgements We are most grateful to the staff of the State Key Laboratory of Geological Processes and Mineral Resources,

China University of Geosciences, Wuhan and the Wuhan Sample Solution Analytical Technology Co., Ltd for their assistance during the U–Pb dating and trace element analyses. Professor Yang Wen and engineer Yu Xihuan from the Hei Longjiang Institute of Geological survey provided great help in field work. We especially thank anonymous reviewers for their insightful and constructive comments. This work was supported by the regional geology and mineralization research program of Heilongjiang province (HLJKD201417).

References

- Atherton MP, Petford N (1993) Generation of sodium-rich magma from newly underplated basaltic crust. *Nature* 362:144–146
- Batchelor RA, Bowden P (1985) Petrogenetic interpretation of granitoid rock series using multicationic parameters. *Chem Geol* 48:43–55
- Castillo PR, Janney PE, Solidum RU (1999) Petrology and geochemistry of Camiguin Island, southern Philippines: insights to the source of adakites and other lavas in a complex arc setting. *Contrib Mineral Petrol* 134:33–51. doi:10.1007/s004100050467
- Chung SL, Liu D, Ji J, Chu MF, Lee HY, Wen DJ et al (2003) Adakites from continental collision zones: melting of thickened lower crust beneath southern Tibet. *Geology* 31:1021–1024. doi:10.1130/G19796.1
- Corfu F, Hanchar JM, Hoskin PWO, Kinny P (2003) Atlas of zircon textures. *Rev Mineral Geochem* 53:469–499
- Davidson J, Turner S, Handley H, Macpherson C, Dosseto A (2007) Amphibole “sponge” in arc crust? *Geology* 35:787–790
- Defant MJ, Drummond MS (1990) Derivation of some modern arc magmas by melting of young subducted lithosphere. *Nature* 347:662–665
- Gao S, Rudnick RL, Yuan HL, Liu XM, Liu YS, Xu WL, Ling WL et al (2004) Recycling lower continental crust in the North China craton. *Nature* 432:892–897
- Ge XY, Li XH, Chen ZG, Li WP (2002) Geochemistry and petrogenesis of Jurassic high Sr/low Y granitoids in eastern China: constraints on crustal thickness. *Chin Sci Bull* 47:962–968
- Ge WC, Wu FY, Zhou CY, Rahman AA (2005) Emplacement age of the Tahe granite and its constraints on the tectonic nature of the Ergun block in the northern part of the Da Hinggan Range. *Chin Sci Bull* 20:2097–2105 (in Chinese)
- Ge WC, Wu FY, Zhou CY, Zhang JH (2007) Porphyry Cu–Mo deposits in the eastern Xing'an–Mongolian orogenic belt: mineralization ages and their geodynamic implications. *Chin Sci Bull* 52:3416–3427 (in Chinese)
- Geng HY, Sun M, Yuan C et al (2009) Geochemical, Sr–Nd and zircon U–Pb–Hf isotopic studies of late Carboniferous magmatism in the West Junggar, Xinjiang: implications for ridge subduction? *Chem Geol* 266:364–389. doi:10.1016/j.chemgeo.2009.07.001
- HBGMR (Hei Longjiang Bureau of Geology and Mineral Resources) (1993) Regional geology of Heilongjiang Province. Geological Publishing House, Beijing (in Chinese with English abstract)
- He ZJ, Li JY, Niu BG, Ren JS (1998) A Late Jurassic intense thrusting-uplifting event in the Yanshan–Yinshan area, Northern China, and its sedimentary response. *Geol Rev* 4:407–418 (in Chinese with English abstract)
- He YS, Li SG, Hoefs J, Huang F et al (2011) Post-collisional granitoids from the Dabie orogen: new evidence for partial melting of a thickened continental crust. *Geochim Cosmochim Acta* 75:3815–3838
- Hu J, Jiang SY, Zhao HX, Shao Y, Zhang ZZ, Xiao E, Wang Y, Dai BZ, Li HY (2012) Geochemistry and petrogenesis of the Huashan granites and their implications for the Mesozoic

- tectonic settings in the Xiaoqinling gold mineralization belt, NW China. *J Asian Earth Sci* 56:276–289
- Hu XL, Ding ZJ, He MC, Yao SZ, Zhu BP, Shen J, Chen B (2014) A porphyry-skarn metallogenic system in the lesser Xing'an Range, NE China: implications from U–Pb and Re–Os geochronology and Sr–Nd–Hf isotopes of the Luming Mo and Xulaojiugou Pb–Zn deposits. *J Asian Earth Sci* 90:88–100
- Huang XL, Xu YG, Lan JB, Yang QJ, Luo ZY (2009) Neoproterozoic adakitic rocks from Mopanshan in the western Yangtze craton: partial melts of a thickened lower crust. *Lithos* 112:367–381
- Innocenti F, Agostini S, Vincenzo GD et al (2005) Neogene and quaternary volcanism in Western Anatolia: magma sources and geodynamic evolution. *Mar Geol* 221:397–421
- Kay RW, Kay SM (1993) Delamination and delamination magmatism. *Tectonophysics* 219:177–189. doi:10.1016/0040-1951(93)90295-U
- Kinny PD, Wijbrans JR, Froude DO, Williams IS, Compston W (1990) Age constraints on the geological evolution of the Narryer Gneiss Complex, Western Australia. *Aust J Earth Sci* 37:51–69
- Koschek G (1993) Origin and significance of the SEM cathodoluminescence from zircon. *J Microsc* 171:223–232
- Kravchinsky VA, Cogné JP, Harbert WP, Kuzmin MI (2002) Evolution of the Mongol-Okhotsk ocean as constrained by new palaeomagnetic data from the Mongol-Okhotsk suture zone, Siberia. *Geophys J Int* 148:34–57
- Li JY (2006) Permian geodynamic setting of Northeast China and adjacent regions: closure of the Paleo-Asian ocean and subduction of the Paleo-Pacific Plate. *J Asian Earth Sci* 26:207–224
- Liu S, Hu RZ, Feng CX, Chi XG, Li C, Yang RH, Wang TW, Jin W (2003) Cenozoic adakite-type volcanic rocks in Qiangtang, Tibet and its significance. *Acta Geol Sin* 77:187–193
- Liu YS, Zong KQ, Kelemen PB, Gao S (2008) Geochemistry and magmatic history of eclogites and ultramafic rocks from the Chinese continental scientific drill hole: subduction and ultra-high-pressure metamorphism of lower crustal cumulates. *Chem Geol* 247:133–153
- Liu YS, Gao S, Hu ZC, Gao CG, Zong KQ, Wang DB (2010) Continental and oceanic crust recycling-induced melt-peridotite interactions in the Trans-North China orogen: U–Pb dating, Hf isotopes and trace elements in zircons from mantle xenoliths. *J Petrol* 51:537–571
- Long X, Wilde SA, Wang Q, Yuan C, Wang XC, Li J, Jiang Z, Dan W (2015) Partial melting of thickened continental crust in central Tibet: evidence from geochemistry and geochronology of Eocene adakitic rhyolites in the northern Qiangtang terrane. *Earth Planet Sci Lett* 414:30–44. doi:10.1016/j.epsl.2015.01.007
- Ludwig KR (2003) User's manual for Isoplot 3.00: a geochronological toolkit for Microsoft Excel. Berkeley Geochronology Center, Berkeley, p 39
- Macpherson CG, Dreher ST, Thirlwall MF (2006) Adakites without slab melting: high pressure differentiation of island arc magma, Mindanao, the Philippines. *Earth Planet Sci Lett* 243:581–593. doi:10.1016/j.epsl.2005.12.034
- Maniar PD, Piccoli PM (1989) Tectonic discrimination of granitoids. *Geol Soc Am Bull* 101:635–643
- Martin H (1986) Effect of steeper Archean geothermal gradient on geochemistry of subduction-zone magmas. *Geology* 14:753–756
- Martin H (1999) The adakitic magmas: modern analogues of Archean granitoids. *Lithos* 46:411–429
- Martin H, Smithies RH, Rapp R, Moyen JF, Champion D (2005) An overview of adakite, tonalite–trondhjemite–granodiorite (TTG), and sanukitoid:relationships and some implications for crustal evolution. *Lithos* 79:1–24
- Maruyama S, Send T (1986) Orogeny and relative plate motions: example of the Japanese Islands. *Tectonophysics* 127:305–329
- Moyen JF, Stevens G (2006) Experimental constraints on TTG petrogenesis: implications for Archean geodynamics. *Geophys Monogr* 164:149–175
- Pearce JA, Harris NBW, Tindle AG (1984) Trace element discrimination diagrams for the tectonic interpretation of granitic rocks. *J Petrol* 25:956–983
- Peccerillo A, Taylor SR (1976) Geochemistry of Eocene calc-alkaline volcanic rocks from the Kastamonu area, northern Turkey. *Contrib Mineral Petrol* 58:63–81
- Pei FP, Xu WL, Yu Y, Zhao QG, Yang DB (2008) Petrogenesis of the late Triassic Mayihe pluton in southern Jilin province: evidence from zircon U–Pb geochronology and geochemistry. *J Jilin Univer (Earth Sci Ed)* 38:252–263 (in Chinese with English abstract)
- Qian Q, Hermann J (2013) Partial melting of lower crust at 10–15 kbar: constraints on adakite and TTG formation. *Contrib Mineral Petrol* 165:1195–1224
- Rapp RP, Watson EB (1995) Dehydration melting of metabasalt at 8–32 kbar: implications for continental growth and crust-mantle recycling. *J Petrol* 36:891–931
- Rapp R, Shimizu N, Norman M, Applegate G (1999) Reaction between slab-derived melts and peridotite in the mantle wedge: experimental constraints at 3.8 GPa. *Chem Geol* 160:335–356
- Rudnick RL, Gao S (2003) Composition of the continental crust. In: Holland HD, Turekian KK (eds) Treatise on geochemistry. The crust, vol 3. Amsterdam, Elsevier, pp 1–64. doi:10.1016/B0-08-043751-6/03016-4
- Sengör AMC, Natal'in BA, Burtman VS (1993) Evolution of the Altai tectonic collage and Palaeozoic crustal growth in Eurasia. *Nature* 364:299–307
- She HQ, Li JW, Xiang AP, Guan JD, Yang YC, Zhang DQ, Tan G, Zhang B (2012) U–Pb ages of the zircons from primary rocks in middle-northern Daxinganling and its implications to geotectonic evolution. *Acta Petrol Sin* 28:571–594 (in Chinese with English abstract)
- Streck MJ, Leeman WP, Chesley J (2007) High magnesian andesite from Mount Shasta: a product of magma mixing and contamination, not a primitive mantle melt. *Geology* 35:351–354. doi:10.1130/G23286A.1
- Sui ZM, Ge WC, Wu FY, Zhang JH, Xu XC, Cheng RY (2007) Zircon U–Pb ages, geochemistry and its petrogenesis of Jurassic granites in northeastern part of the Da Hinggan Mts. *Acta Petrol Sin* 23:461–480 (in Chinese with English abstract)
- Sun SS, McDonough WF (1989) Chemical and isotopic systematics of oceanic basalts: implications for mantle composition and processes, vol 42. Geological Society, Special Publications, London, pp 313–345
- Sun DY, Suzuki K, Wu FY, Lu XP (2005) CHIME dating and its application for Mesozoic granites of Huanggoushan, Jilin Province. *Geochimica* 34:305–314 (in Chinese with English abstract)
- Sylvester PJ (1998) Post-collisional strongly peraluminous granites. *Lithos* 45:29–44. doi:10.1016/S0024-4937(98)00024-3
- Tomurtogoo O, Windley BF, Kröner A, Badarch G, Liu DY (2005) Zircon age and occurrence of the Adaatsag ophiolite and Muron shear zone, central Mongolia: constraints on the evolution of the Mongol-Okhotsk ocean, suture and orogen. *J Geol Soc Lond* 162:125–134
- Wang Q, Wyman DA, Xu JF, Jian P, Zhao ZH, Li CH, Xu W (2007) Early Cretaceous adakitic granites in the Northern Dabie Complex, central China: implications for partial melting and delamination of thickened lower crust. *Geochim Cosmochim Acta* 71:2609–2636
- Watson EB, Harrison TM (1983) Zircon saturation revisited: temperature and composition effects in a variety of crustal magma types. *Earth Planet Sci Lett* 64:295–304

- Wiedenbeck M, Alle P, Corfu F, Griffin WL, Meier M, Oberli F, Quadt A, Roddick JC, Spiegel W (1995) Three natural zircon standards for U–Th–Pb, Lu–Hf, trace element and REE analyses. *Geostand Geoanal Res* 19:1–23
- Wilde SA, Dorsett-Bain HL, Liu JL (1997) The identification of a Late Pan-African granulite facies event in northeastern China: SHRIMP U–Pb zircon dating of the Mashan Group at Liu Mao, Heilongjiang Province, China. In: Proceedings of the 30th IGC: Precambrian Geology and Metamorphic Petrology, vol 17. VSP International Science Publishers, Amsterdam, pp 59–74
- Williams IS, Claesson S (1987) Isotopic evidence for the Precambrian provenance and Caledonian metamorphism of high grade paragneisses from the Seve Nappes, Scandinavian Caledonides: II. Ion microprobe zircon U–Th–Pb. *Contrib Mineral Petrol* 97:205–217
- Wolf MB, Wyllie PJ (1994) Dehydration-melting of amphibolite at 10 kbar: the effects of temperature and time. *Contrib Mineral Petrol* 115:369–383
- Wu FY, Sun DY, Li HM, Jahn BM, Wilde S (2002) A-type granites in northeastern China: age and geochemical constraints on their petrogenesis. *Chem Geol* 187:143–173
- Wu G, Sun FY, Zhao CS, Li ZT, Zhao AL, Pang QB, Li GY (2005) Discovery of the Early Paleozoic post-collisional granites in northern margin of the Ergun massif and its geological significance. *Chin Sci Bull* 50:2733–2743 (in Chinese)
- Wu FY, Zhao GC, Sun DY, Wilde SA, Yang JH (2007) The Hulan Group: its role in the evolution of the Central Asian orogenic belt of NE China. *J Asian Earth Sci* 30:542–556
- Wu FY, Sun DY, Ge WC, Zhang YB, Grant ML, Wilde SA, Jahn BM (2011) Geochronology of the Phanerozoic granitoids in northeastern China. *J Asian Earth Sci* 41:1–30
- Wu G, Chen YC, Chen YJ, Zeng QT (2012) Zircon U–Pb ages of the metamorphic supracrustal rocks of the Xinhudukou Group and granitic complexes in the Argun massif of the northern Greater Xing'an Mountains, NE China, and their tectonic implications. *J Asian Earth Sci* 49:214–233
- Wyllie PJ, Wolf MB (1993) Amphibolite dehydration-melting: sorting out the solidus. Geological Society, London, Special Publications 76:405–416
- Xiao WJ, Windley BF, Hao J, Zhai MG (2003) Accretion leading to collision and the Permian Solonker suture, Inner Mongolia, China: termination of the Central Asian orogenic belt. *Tectonics* 22:8–1–20
- Xu JF, Shinjo R, Defant MJ, Wang Q, Robert P (2002) Origin of Mesozoic adakitic intrusive rocks in the Ningzhen area of east China: partial melting of delaminated lower continental crust? *Geology* 30:1111–1114
- Xu WL, Wang QH, Wang DY, Guo JH, Pei FP (2006) Mesozoic adakitic rocks from the Xuzhou–Suzhou area, eastern China: evidence for partial melting of delaminated lower continental crust. *J Asian Earth Sci* 27:454–464
- Xu WL, Herdt JM, Gao S, Pei FP, Wang W, Yang DB (2008) Interaction of adakitic melt-peridotite: implications for the high-Mg# signature of Mesozoic adakitic rocks in the eastern North China Craton. *Earth Planet Sci Lett* 265:123–137
- Xu HJ, Ma CQ, Zhang JF, Ye K (2013) Early Cretaceous low-Mg adakitic granites from the Dabie orogen, eastern China: petrogenesis and implications for destruction of the over-thickened lower continental crust. *Gondwana Res* 23:190–207
- Yang DB, Xu WL, Zhao GC, Huo TF, Shi JP, Yang HT (2016) Tectonic implications of Early Cretaceous low-Mg adakitic rocks generated by partial melting of thickened lower continental crust at the southern margin of the central North China Craton. *Gondwana Res* 38:220–237
- Yin A, Nie S (1996) A Phanerozoic palinspastic reconstruction of China and its neighboring regions. In: Yin A, Harrison TM (eds) The tectonic evolution of Asia. Cambridge University Press, Cambridge, pp 442–485
- Ying JF, Zhou XH, Zhang LC, Wang F (2010) Geochronological framework of Mesozoic volcanic rocks in the Great Xing'an Range, NE China, and their geodynamic implications. *J Asian Earth Sci* 39:786–793
- Zhang Q, Wang Y, Qian Q, Yang JH, Wang YL, Zhao TP, Guo GJ (2001) The characteristics and tectonic–metallogenic significances of the adakites in Yanshan period from eastern China. *Acta Petrol Sin* 17:236–244
- Zhang JH, Gao S, Ge WC, Wu FY, Yan JH, Wilde SA, Li M (2010) Geochronology of the Mesozoic volcanic rocks in the Great Xing'an Range, Northeastern China: implications for subduction-induced delamination. *Chem Geol* 276(3):144–165
- Zhao X, Coe RS, Zhou Y, Wu H, Wang J (1990) New paleomagnetic results from northern China: collision and suturing with Siberia and Kazakhstan. *Tectonophysics* 181:43–81
- Zhao CJ, Peng YJ, Dang ZX, Zhang YP, Zhu Q, Shu YZ, Wang ZF, Tai CB, Gu F, Zhang JF, Zheng CZ, Dang YS (1996) Tectonic Framework and crust evolution of eastern Jilin and Heilongjiang provinces. Publishing House of Liaoning University, Shenyang, p 186 (in Chinese with English abstract)
- Zhou JB, Wilde SA, Zhang XZ, Zhao GC, Zheng CQ, Wang YJ, Zhang XH (2009) The onset of Pacific margin accretion in NE China: evidence from the Heilongjiang high-pressure metamorphic belt. *Tectonophysics* 478:230–246
- Zhou JB, Wilde SA, Zhang XZ, Ren SM, Zheng CQ (2011) A >1300 km late Pan-African metamorphic belt in NE China: new evidence from the Xing'an block and its tectonic implications. *Tectonophysics* 509:280–292
- Zhou XC, Zhang HF, Luo BJ, Pan FB, Zhang SS, Guo L (2016) Origin of high Sr/Y-type granitic magmatism in the southwestern of the Alxa block, Northwest China. *Lithos* 256–257:211–227